The liquid metal embrittlement of a reactive system at room temperature: α-brasses in contact with the liquid eutectic Ga-In

Marco Ezequiel, Ingrid Proriol Serre, Thierry Auger, Eva Héripré, Zehoua Hadjem-Hamouche, Loïc Perriere

Engineering Failure Analysis 164 (2024) 108694

Contents lists available at ScienceDirect

Engineering Failure Analysis

journal homepage: www.elsevier.com/locate/engfailanal

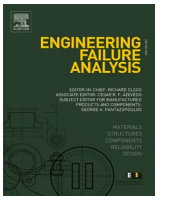

The liquid metal embrittlement of a reactive system at room temperature: α-brasses in contact with the liquid eutectic Ga-In

Marco Ezequiel [a,*], Ingrid Proriol Serre [a,*], Thierry Auger [b], Eva Héripré [b,c], Zehoua Hadjem-Hamouche [b], Loïc Perriere [d]

[a] Univ. Lille, CNRS, INRAE, Centrale Lille, UMR 8207 – UMET – Unité Matériaux et Transformations, F-59000 Lille, France
[b] PIMM Laboratory, Arts et Métiers Institute of Technology, CNRS, CNAM, HESAM University, 151 boulevard de l'Hôpital, 75013 Paris, France
[c] Université Paris-Saclay, CentraleSupélec, ENS Paris-Saclay, CNRS, LMPS – Laboratoire de Mécanique Paris-Saclay, 91190 Gif-sur-Yvette, France
[d] Institut de Chimie et des Matériaux de Paris Est, UMR 7182, CNRS – Université Paris-Est, Thiais, France

ARTICLE INFO

Keywords:
Liquid metal embrittlement
α-brasses
Gallium-indium eutectic
In situ observation
Finite element analysis
Wetting

ABSTRACT

We studied the liquid metal embrittlement (LME) at room temperature of α-brasses by the liquid eutectic Ga-In (EGaIn). The EGaIn partially wets the α-brasses and forms the $CuGa_2$ intermetallic. 3-point bending tests, Finite Element Analysis, and in situ testing were conducted. When LME occurs, there is a ductile fracture followed by an intergranular brittle fracture that propagates through the zones with the highest plastic strain. The LME sensitivity increases with higher strain rates, higher Zn content, and higher work hardening rates, suggesting a significant role of dislocation mobility in LME and a lack of influence from the $CuGa_2$ intermetallic.

1. Introduction

Liquid Metal Embrittlement (LME) is a phenomenon that can occur when a solid metal or alloy undergoes plastic deformation in contact with a liquid metal or alloy. Its main effect is a detrimental change in the mechanical properties of the solid. This phenomenon does not usually affect the elastic behaviour of the solid; instead, it generates a loss of ductility, a premature fracture, or a change in the fracture mode [1–4]. Because of the detrimental effects on solids, the study of LME concerns many fields, such as soldering/welding, heat-resistant alloys, and nuclear and military applications [3,5–7].

Several mechanisms and models have been proposed to explain and predict the LME phenomenon; their surveys are available in the literature [8–10]. However, these are limited in the range of conditions and systems they can correctly describe. The lack of a model that can explain all LME cases comes from the phenomenon complexity, the limited experimental data, and the differences in the mechanisms for each solid/liquid couple [4,10,11]. For instance, there is not much information on reactive systems, which could give valuable insights into this phenomenon while also impacting the understanding of LME in industrial cases such as Fe/Zn [7]. Additionally, there are no reported in situ observations of LME, so the interpretation of the phenomenon relies purely on post-mortem observations.

The LME prediction is difficult because of its strong dependence on several material properties and the testing conditions [3,12,13]. Materials with a higher work hardening rate generally present more severe LME, e.g., T91 steel in contact with the lead–bismuth eutectic (LBE) [14]. The strain rate at which the solid metal undergoes plastic deformation can influence the LME; high strain rates

* Corresponding authors.
E-mail addresses: marco.ezequiel@lspm.cnrs.fr (M. Ezequiel), ingrid.proriol-serre@univ-lille.fr (I. Proriol Serre).

https://doi.org/10.1016/j.engfailanal.2024.108694
Received 4 June 2024; Received in revised form 12 July 2024; Accepted 19 July 2024
Available online 22 July 2024

often increase LME [11,15]; e.g., in the Bi/Cu system, the crack propagation rate increases almost linearly with the increase of the strain rate [16]. However, the T91 steel in contact with the LBE presents higher LME sensitivity at lower strain rates [17], which may be explained by a competition between bulk and surface effects [18].

An apparent requirement for LME is good contact conditions between the liquid and the solid. If this contact is interrupted, LME will not happen or stop if it has already started. Therefore, oxide films and intermetallics play a role in LME since they can modify the contact between the liquid and the solid [3,11,19–21]. Some works claim that there should be no intermetallic formation between the metals during the contact for LME to happen [2,15]. Nonetheless, Clegg and Jones reported the appearance of LME despite the intermetallics in En19 steel/Sn [22]. However, they did not describe the role of intermetallics on LME sensitivity, and the study focused on steel dissolution in Sn. In contrast, Glikman and Goryunov reported that the intermetallic could change the crack growth kinetics in the case of Cu embrittled by Bi [23]. They reported that when there is an addition of Sb to the liquid Bi, there are compounds formed between Cu and Sb that generate a discontinuous crack growth with stops, which correspond to the rupture and reformation of the Cu-Sb intermetallics.

A widely studied reactive system that presents LME is Fe in contact with liquid Zn. In this system, the formation of the intermetallics drastically changes the ductile-to-brittle transition strain-rate dependence. Kang et al. explain this relation by stating that whenever there is enough time to form intermetallics with a melting point higher than pure Zn, there will not be any available liquid metal to trigger LME [7].

Studying reactive systems at room temperature can lead to a better understanding of LME since the practical limitations for the testing are reduced. For instance, a reactive system prone to LME consists of Cu-Zn alloys in contact with the eutectic Ga-In (EGaIn), where Cu reacts with Ga to form the $CuGa_2$ intermetallic at room temperature and Cu_9Ga_4 at temperatures above 90 °C [24].

Fernandes and Jones studied the tensile mechanical properties of Cu-30 %Zn in contact with liquid Ga, which is liquid at 30 °C [25]. They reported no evidence of LME under any conditions tested and that all specimens presented a ductile fracture with signs of microvoid coalescence. They further repeated the tensile tests on notched brass specimens and observed a diminution in the degree of plastic deformation at fracture and the magnitude of the fracture stress. On those specimens, they observed a brittle intergranular cracking. However, neither this study nor any other LME studies of Cu-Zn alloys in contact with Ga-based liquid alloys report any role of the intermetallic in the LME sensitivity [12,21,25]. In the literature, Lukowski et al. are the only ones to mention the role of a Cu-Ga reaction on the LME of β-brass in contact with Ga [26]. They reported that the non-uniform interaction between Ga and the β-brass generates the crack to propagate in a series of jumps.

This work aims to study the embrittlement of Cu and α-brasses in contact with the liquid eutectic Ga-In (EGaIn) to deepen the understanding of the LME phenomenon at room temperature on reactive couples. The α-brasses are monophasic alloys with no precipitation of second phases and relatively simple microstructure; these characteristics simplify the interpretation of the results and allow a clearer understanding of the phenomena involved, additionally allowing the comparison of different composition without the complexity related to a change of microstructure. The EGaIn is liquid at room temperature, is not toxic, and has a low vapour pressure; these characteristics expand the experimental possibilities since there is no need for heating devices or special precautions in handling the liquid metal, and it does not emit vapour when in vacuum.

α-brasses with different Zn contents were considered in this study. The contact conditions between them and the EGaIn were quantified by measuring the contact angle. Miniaturised bending tests were carried out under different strain rates and various metallurgical states of the alloys with different Zn contents to characterise the possible effects of these parameters on the LME sensitivity. Also, the LME phenomenon was observed punctually in situ using a Scanning Electron Microscope (SEM). Additionally, the mechanical conditions of the sample during the tests were calculated using the Finite Element Method (FEM) to relate them with the LME appearance. These effects are associated with the different parameters, the $CuGa_2$ intermetallic, and the possible mechanisms

Table 1
Hardness and grain size of the materials tested.

Material	Condition	Hardness (HV)	Grain size (μm)	Setup used
Cu	As-received	100	20	1 & 2
Cu-15 %Zn	As-received	75	20	1 & 2
	Rolled at 10 %	120	20	2
Cu-20 %Zn	As-received	212	Not measured	1
	Annealed 300 °C – 2 h	133	Not measured	1
Cu-25 %Zn	As-received	210	Not measured	1
	Annealed 300 °C – 2 h	133	Not measured	1
	Annealed 350 °C – 2 h	109	Not measured	1
Cu-30 %Zn	As-received	142	39	1
	Annealed 380 °C – 2 h	115	40	1
	As-received	151	20	2
	Annealed 350 °C – 0.75 h	124	20	2
	Annealed 350 °C – 1.5 h	78	16	2

behind the LME.

2. Materials and methods

2.1. Properties of the tested materials

Alloys with different Zn contents were tested to highlight the effect of the Zn content on the liquid metal embrittlement (LME). Additionally, some were heat treated to change their metallurgical conditions to study the impact of the work hardening rate on the LME susceptibility. Table 1 summarises the materials tested and their corresponding metallurgical states; it also shows with which testing setup they were tested. The setups are explained in the second part of this section. The hardness of the materials was measured with a Buelher hardness testing machine, and the grain size was measured by optical microscopy using the linear intercept method on samples mechanically polished with SiC papers and diamond paste and then etched.

Pure Cu and the Cu-30 %Zn alloy were supplied by the commercial group Alfa Aesar, while the Cu-15 %Zn alloy was supplied by Wieland. In contrast, the Cu-20 %Zn and Cu-25 %Zn alloys were not commercially available; thus, they were elaborated in the Institut de Chimie et des Matériaux Paris-Est (ICMPE) by using an induction furnace to melt 99.99 % purity Cu and 99.95 % purity Zn in a glassy carbon crucible to produce cylinders with a diameter of 12 mm and height of 8 mm. These were then cross-rolled until achieving a thickness of 2 mm. The elaboration processes of these alloys introduced a high level of deformation, yielding Cu-20 %Zn and Cu-25 % Zn samples with high hardness values, indicating a high work hardening rate. The high deformation of their microstructures made it impossible to measure the grain size, even after the annealing heat treatment.

The EGaIn used in this work was prepared using 99.99 % pure Ga supplied by Mining & Chemical Products and 99.99 % pure In provided by Alfa Aesar. A hot plate was used to heat water in a beaker to approximately 80 °C; the bottle containing Ga was introduced into the beaker until Ga melted. Liquid Ga was then poured into a ceramic crucible, and the In was added until the mixture attained the EGaIn composition, i.e., 24.5 %wt. In. The mix was stirred until it was a homogeneous liquid. A RAININ micropipette with a 2–20 μL capacity was used to manipulate the liquid metal.

2.2. Experimental methods

The contact angle between the liquid EGaIn and the different solids was measured to quantify the contact conditions. Before the measurements, a 1 M HCl aqueous solution was used to deoxidise the surface of the solid and the liquid EGaIn [27–29]. A Krüss DSA100 drop analyser was used for the measurements. Instead of the automatised dosing unit incorporated in the machine, a RAININ micropipette with a capacity of 2–20 μL was used to place the drop on the solid sample just before the measurement. The solid samples tested were previously metallographically prepared using SiC abrasive paper and 6, 3, and 1 μm diamond paste. A Bruker Contour GT-K 3D Optical Microscope was used to verify the low roughness of the samples. All average absolute values of the profile heights (Ra) [30] were consistently below 20 nm. The open-source image processing package FIJI and the Contact Angle plugin were used to measure the contact angle [31,32]. The time between the deoxidisation and the drop placement was always below 5 min, which is far less than the lower limit for the regrowth of the oxide layer, estimated by a preliminary study. At least 12 contact angles were measured for each of the compositions.

The samples were mechanically tested using the 3-point bending test, which is easily miniaturised and allows the screening of several testing conditions using little material. Moreover, this test presents a higher stress magnitude on the sample surface, making it ideal for studying the LME. For comparison, in the case of standard tensile tests, the strain develops homogenously along the whole specimen, but only the surface is in contact with the liquid metal. In the case of the studies of the LME using tensile tests, the strain distribution leads to a competition between the fracture that may initiate in the bulk of the sample and the fracture that may initiate in its surface. Hemery et al. presented an example of this competition in the T91 steel tested in contact with liquid sodium [33].

In this work, the mechanical tests were done at room temperature, taking advantage of the low melting point of the EGaIn (15.5 °C)

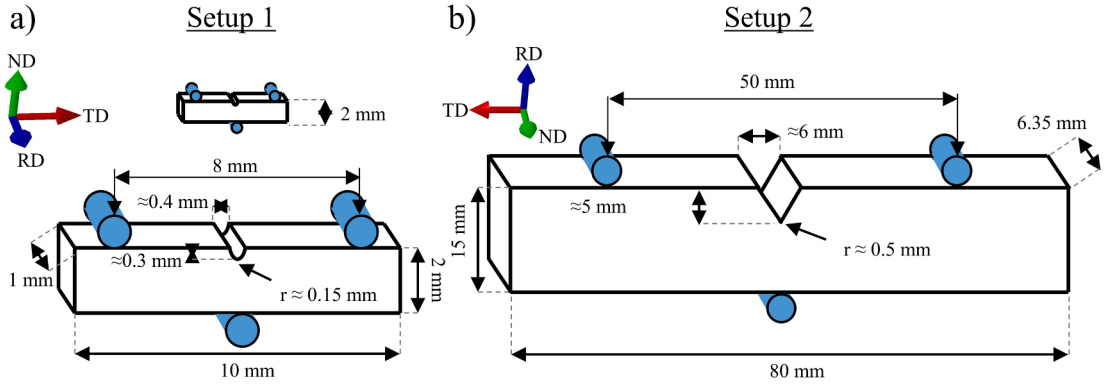

Fig. 1. Sample geometries for a) Setup 1 and b) Setup 2 used for the 3-point bending tests.

[34]. To test different mechanical conditions and strain rates, two different 3-point bending test setups were used along with varying displacement rates. Fig. 1 shows the sample geometry and dimensions that correspond to both setups and indicates the samples rolling direction (RD), transversal direction (TD), and normal direction (ND). The samples, including the notch, were manufactured by wire electrical discharge machining (WEDM). The radius of the notch was measured by optical microscopy. Concerning Setup 1, due to the small dimensions of these samples, there were slight misalignments from test to test, which generated subtle differences in the force–displacement curves; however, these variations are not significant enough to override the eventual effect of the liquid EGaIn on the mechanical properties of the solid metal or alloy.

These different setups allow the obtention of different strain rates and stress magnitudes. The small dimensions of Setup 1 allow us to screen a broader range of conditions. Still, it presents the disadvantage that the supports can move a shorter distance, thus limiting the quantity of strain introduced to the sample. This disadvantage is reduced in Setup 2; also, the higher dimensions of Setup 2 lead to higher strain rates.

For Setup 1, a 5567A Instron Universal Testing Machine with a force cell of 30 kN was used in compression mode. At least two samples were tested for each combination of material, condition, displacement rate, and environment. The curves presented repeatability, so only one curve was chosen randomly per condition to be plotted in the results. For Setup 2, an Instron 5581 with a force cell of 50 kN was used, and one sample was tested per condition.

The samples and the liquid EGaIn were deoxidised using 1 M HCl and then placed in contact minutes before the bending tests; a visual confirmation that the liquid EGaIn entered the sample notch was done with the naked eye before each test.

Several studies show that the $CuGa_2$ intermetallic compound forms whenever Cu or α-brasses are in contact with the EGaIn at room temperature [24,34]. This intermetallic can be observed by scanning electron microscopy (SEM) after removing the liquid EGaIn from the solid surface. The EGaIn can be removed by immersing the sample in a 1.1 M aqueous solution of HNO_3 while simultaneously immersing the solution in an ultrasonic bath. The SEM images in Fig. 2 show the presence of the $CuGa_2$ compound on a Cu-30 %Zn sample.

Energy-dispersive X-ray (EDX) and Inductively Coupled Plasma-Optical Emission Spectroscopy (ICP-OES) analyses confirmed that the observed intermetallic is $CuGa_2$ [35]. Moreover, removing the intermetallic compound from the surface is possible by submerging the samples in a 1 M aqueous solution of NaOH while simultaneously immersing the solution in an ultrasonic bath. This methodology is used to observe the fracture surfaces presented in this work.

Micrographies were obtained using a Hitachi SU 5000 SEM with an Oxford Symmetry EBSD camera and a Bruker Quantax EDX detector in the electron microscopy facility of the Advanced Characterization Platform of the Chevreul Institute. In this work, all the micrographies correspond to images taken using the secondary electron detector. This microscope was also used to characterise some samples by electron backscattering diffraction (EBSD).

An additional real-time test was done with observations in situ using the same SEM. For this, a Deben MICROTEST machine was used to test samples using the dimensions of Setup 1 (Fig. 1). The displacement rate of this test was 0.4 mm/min. During the 3-point bending tests, a video was recorded using the secondary electron detector with an image acquisition of 30 fps. For clearer image acquisition, one face of each sample tested in situ was previously polished manually using SiC abrasive paper and diamond pastes with different granulometry down to ¼ μm. Then, the samples were etched using an aqueous solution of $FeCl_3$ and HCl to reveal the grain boundaries.

2.3. Numerical methods

The ABAQUS 6.13 software was used to perform finite element modelling of the tests corresponding to Setup 1. Fig. 3a shows the assembly that simulates the 3-point bending tests with the correspondent mesh and boundary conditions. Only a quarter part of the specimen was modelled, taking advantage of the two planes of symmetry of the sample. These symmetry conditions correspond to the movement restriction in the TD direction of the nodes in one of the ND-RD faces and the same restriction in the RD direction for the nodes in one of the ND-TD faces. The lower support movement is restrained, and the movement of the upper support is set to a negative displacement in the ND direction. Both supports were modelled as rigid bodies, and a frictionless tangential behaviour was considered between the specimen and the supports. There is a total of 25,720 degrees of freedom in the model.

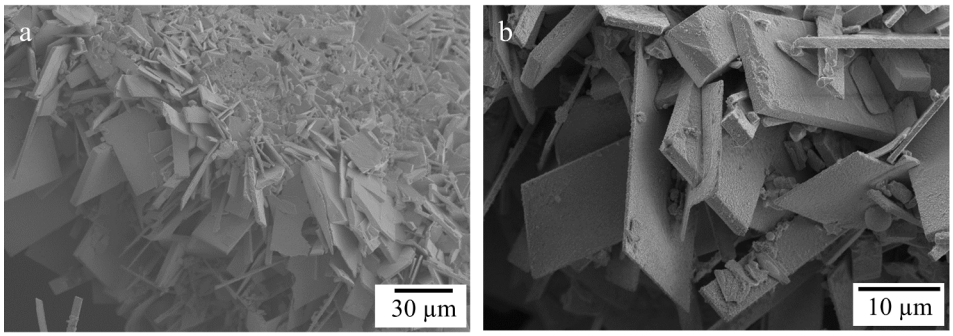

Fig. 2. $CuGa_2$ intermetallic that forms whenever the Cu-30%Zn brass enters contact with the EGaIn.

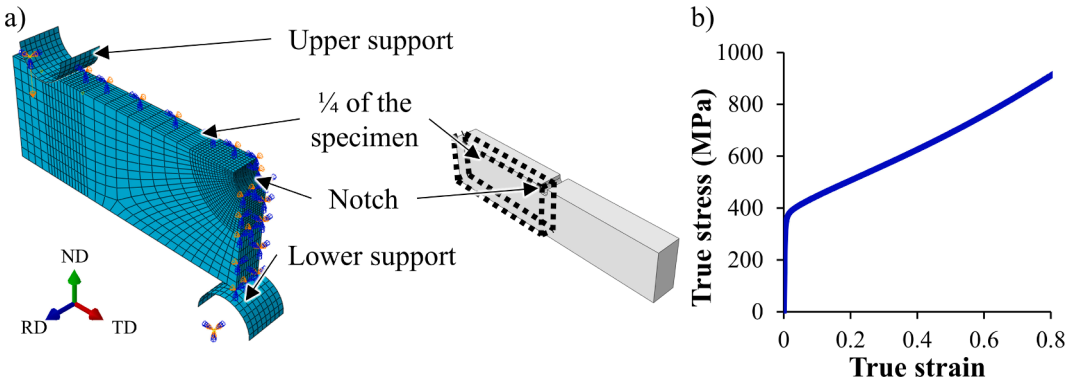

Fig. 3. A) assembly used to simulate the 3-point bending test on a quarter part of the miniaturised specimen, boundary conditions and mesh included, and b) true stress-true strain curve of the cu-30%zn implemented in the simulation.

The only material implemented in the model was the Cu-30 %Zn alloy. To describe its mechanical behaviour, tensile tests were carried out in flat specimens combined with digital image correlation (DIC) to accurately obtain the material true stress-true strain curve (Fig. 3b). A Young's modulus of 99.7 GPa was derived from this curve, and the experimental true plastic strain-true stress data was directly fed into the software, considering an isotropic mechanical behaviour. The Poisson's ratio was set to 0.33.

The FEM was used to estimate the nucleation and growth of the microvoids in the material, which are phenomena that lead to the rupture of the Cu-30 %Zn alloy. For the modelling of these phenomena, the Gurson-Tvergaard-Needleman (GTN) model was implemented in the analysis; more details of the implementation of this model on a FEM using ABAQUS can be found elsewhere [36,37]. The initial relative density value was considered to be 1. The coefficients q_1, q_2, and q_3 were set to 1.5, 1 and 2.25, respectively. The other material constants necessary for this modelling were obtained by simulating the tensile tests using initial values obtained from the literature [37]: ε_N=0.3, S_N=0.1, and f_N=0.02. The force and displacement values were obtained from the simulations and then compared with the experimental data of the tensile test. The values of the materials constants were iteratively adjusted manually to fit the experimental curve. The optimised values of the parameters of the GTN model for Cu-30 %Zn that are further used in this work are ε_N=0.45, S_N=0.25, and f_N=0.012. A mesh sensitivity study was carried out to confirm the independence of the mesh size with the results obtained.

3. Experimental results

This section will first evaluate whether there are good contact conditions between the different brasses and the liquid EGaIn, which is necessary for LME to occur. Then, the section will present the specific impact of LME on the mechanical properties of the different brasses. The mechanical testing results are arranged to highlight the spectrum of LME sensitivity across the alloys, from the most to the least affected, to help comprehensively understand the effect of the LME on these alloys.

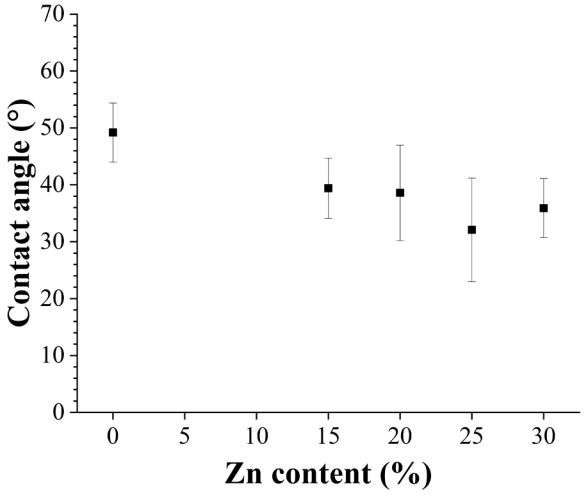

Fig. 4. Evolution of the contact angle with Zn content of Cu-Zn alloys in contact with liquid EGaIn.

3.1. Contact conditions of Cu and α-brasses with the liquid EGaIn

The contact conditions of the different alloys with the liquid EGaIn are quantified by measuring the contact angle; Fig. 4 shows these measurements. There is partial wettability in all the solid compositions since the contact angle is greater than 0. Still, it is in good wetting conditions with contact angle values consistently below 60°. Moreover, there is a slight tendency to a lower contact angle as the Zn content increases, indicating that in these alloys, Zn enhances the wetting capacity of the liquid EGaIn.

The dispersion in the contact angle was considerable for all compositions. This dispersion could be related to the contact angle hysteresis caused by the reaction between the solid and the liquid or by the liquid metal oxide layer. Since both phenomena may not change significantly with the composition of the solid, in this range of compositions, the contact angle hysteresis does not change significantly with the composition. However, it was still impossible to measure the contact angle hysteresis by tilting the platform since there is an immediate reformation of the oxide layer in the liquid that impedes the movement of the drop. This oxide layer impedes the change of contact angle even at high tilt angles.

3.2. Mechanical testing of Cu-30 %Zn in contact with the liquid EGaIn

In this study, an important focus was placed on the Cu-30 %Zn since the results showed that this alloy has a higher sensitivity to LME in contact with the liquid EGaIn. Cu-30 %Zn samples with two different metallurgical conditions were tested with Setup 1 in air and in contact with the liquid EGaIn at four different displacement rates; Fig. 5 shows the correspondent force–displacement curves. For both metallurgical conditions, the displacement at failure is consistently lower in the samples tested in contact with the liquid EGaIn. These samples also presented a sudden load decrease, contrary to the samples tested in the air, which showed a steady force decrease. The sudden force drop indicates a fracture requiring very little energy to propagate.

The differences between the mechanical behaviour of the samples tested in air and those tested in contact with the liquid EGaIn are only present in the last part of the curve, indicating that the liquid EGaIn does not change the material elastic or plastic behaviour before failure. Moreover, the point of maximum load is similar whether the samples are tested in air or in contact with the liquid metal. This indicates that the fracture behaviour divergence between the samples tested in air and those tested in contact with the liquid EGaIn appears during the crack propagation stage.

Cu-30 %Zn samples with different metallurgical states were also tested with Setup 2 in air and in contact with the liquid EGaIn at different displacement rates; Fig. 6 summarises the correspondent load–displacement curves. The curves show that the presence of liquid EGaIn modifies the mechanical behaviour of the Cu-30 %Zn samples. However, when testing with Setup 2, some of the samples tested in contact with the liquid EGaIn presented a force drop at the beginning of the plastic regime, indicating no significant plastic deformation before the final failure. This behaviour was observed at all displacement rates tested for the as-received samples and the samples annealed at 350 °C for 0.75 h, except for the tests done at a 1 mm/min displacement rate. In these two metallurgical conditions, fast crack propagation is evidenced by the sudden force drop in the curve.

Fig. 6c shows that the mechanical behaviour of the Cu-30 %Zn samples annealed at 350 °C for 1.5 h presents some differences with the other samples. The divergence in the mechanical behaviour of the samples tested in air and those tested in contact with the liquid EGaIn appears after significant plastic deformation. Also, there is no sudden decrease of the force but a steady decrease at the displacement rate of 100 and 10 mm/min, and an alternation of sudden drops of the force and steady decreases at a 1 mm/min displacement rate.

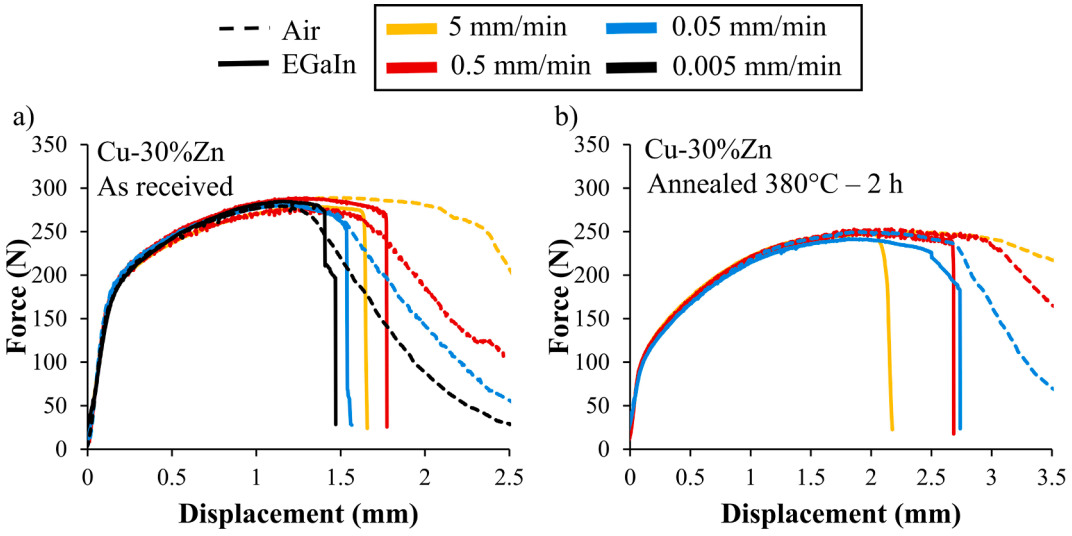

Fig. 5. Force-displacement curves of Cu-30%Zn samples tested in air and in contact with the liquid EGaIn using the 3-point bending test with Setup 1 at different displacement rates.

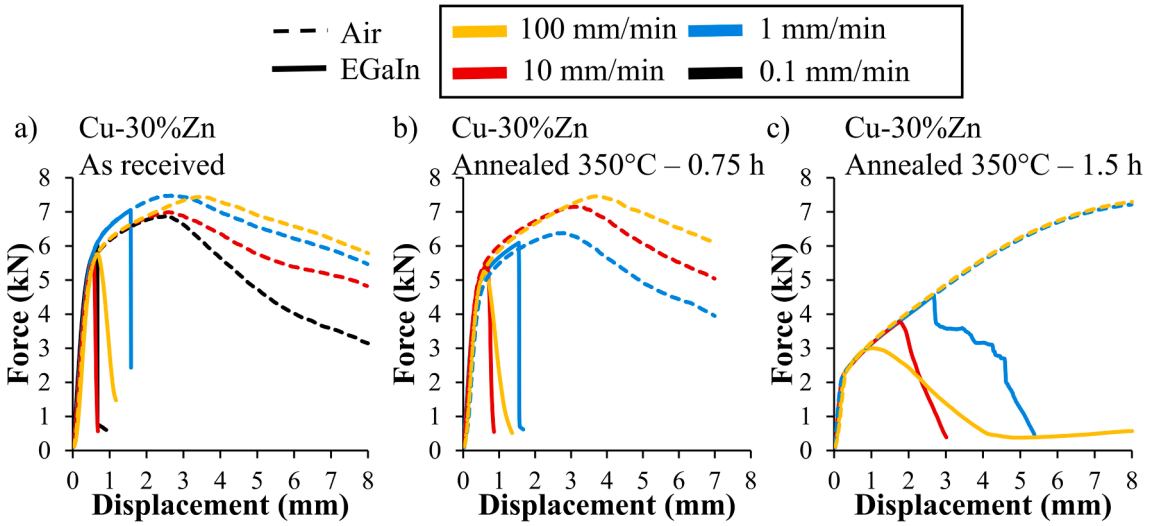

Fig. 6. Force-displacement curves of Cu-30%Zn samples tested in air and in contact with the liquid EGaIn using the 3-point bending test with Setup 2 at different displacement rates.

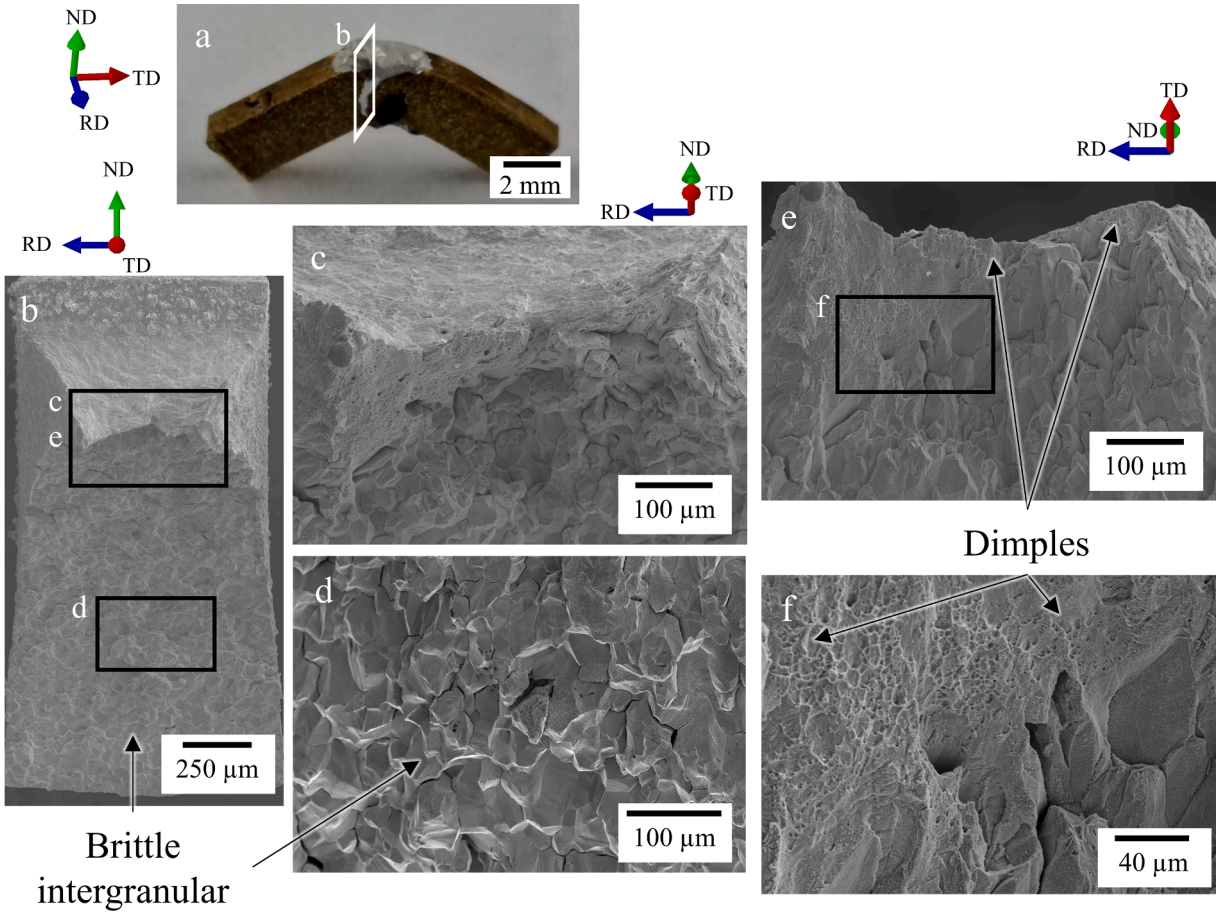

Fig. 7. Cu-30 %Zn as-received sample tested in contact with the liquid EGaIn using the 3-point bending test with Setup 1 at a 5 mm/min displacement rate. a) Sample with the liquid EGaIn, b-d) fractographies after cleaning with HNO_3 and NaOH.

To further understand the effect of the liquid EGaIn on the failure of the samples, some of the fracture surfaces of the Cu-30 %Zn samples tested with Setup 1 were analysed. In the first instance, the fractures of the samples tested in air were observed, and they presented a ductile fracture, evidenced by ductility dimples, which is expected for this material. In contrast, the fractures of the samples tested in contact with the liquid EGaIn at the same conditions present a brittle intergranular fracture on most of its surface, as exemplified in Fig. 7 for a sample tested at a 5 mm/min displacement rate. Furthermore, these samples present a zone at the beginning of the fracture where there are ductile characteristics, i.e., ductility dimples. Fig. 7e shows the short transition zone from a ductile to a brittle fracture, which matches the behaviour observed in the force–displacement curves, i.e., the embrittlement by the liquid EGaIn appears during the propagation of an existent fracture.

Another sample tested at 5 mm/min in contact with the liquid EGaIn was cut transversally for observation by SEM to further characterise the fracture behaviour. Fig. 8 presents the correspondent micrographies and electron backscattering diffraction (EBSD) analysis. The beginning of the fracture shows high plastic deformation of the material, evidenced by the elongated grains in the TD direction, which is the direction of the highest tensile stress. The degree of plastic deformation matches the observation of the ductile fracture; this zone is approximately 200 μm long. In contrast, further from this zone, there is no considerable plastic deformation and the fracture propagates through the grain boundaries, indicating a brittle intergranular fracture propagation.

Regarding fracture propagation, the fracture of the samples tested in air initiates at the bottom of the notch. It propagates in the plane perpendicular to TD, a standard fracture propagation of a ductile material. Fig. 7 and Fig. 8 show that the samples tested in contact with the liquid EGaIn present a ductile fracture that similarly propagates perpendicularly to TD, but in contrast with the samples tested in air, this fracture is immediately followed by a brittle fracture that starts its propagation in the plane perpendicular to ND and then transitions to propagation in the plane perpendicular to TD. Moreover, the Cu-30 %Zn samples tested with Setup 1 presented the same fracture behaviour regardless of the displacement rate of the test.

To better illustrate this particular fracture behaviour, we present in situ observations of a 3-point bending test with liquid EGaIn at a displacement rate of 0.4 mm/min, following the methodology explained previously. Figure 9 illustrates key moments of the test: (a) the initial presence of the liquid EGaIn in the sample notch, (b) the ductile fracture initiation, (c) an early stage of the ductile fracture propagation, which is filled with the liquid EGaIn, and (d) the last moment before the appearance of the sudden brittle fracture. Finally, Fig. 9e shows the moment of sudden force decrease, which is accompanied by a sudden brittle fracture propagation that goes across the totality of the sample. During the initial ductile fracture, there is considerable plastic deformation, and the grains elongate. In contrast, no further plastic deformation occurs once the brittle fracture appears. These results match with those observed post-mortem (Fig. 8).

Using the in situ observations, it is possible to estimate the crack rate at the corresponding displacement rate (0.4 mm/min). Considering that 176 s elapsed between the first fracture appearance (Fig. 9b) and the sudden failure (Fig. 9d) and estimating a crack advance of 200 μm, the average crack rate of the ductile fracture is 1.14 μm/s. Using the same reasoning between the start (Fig. 9d) and the end (Fig. 9e) of the brittle fracture propagation, the calculated average crack rate for the brittle fracture was 2400 μm/s. However, the time between points d and e in Fig. 9 is constrained by the data acquisition time, so the real brittle crack rate should be higher than the estimation.

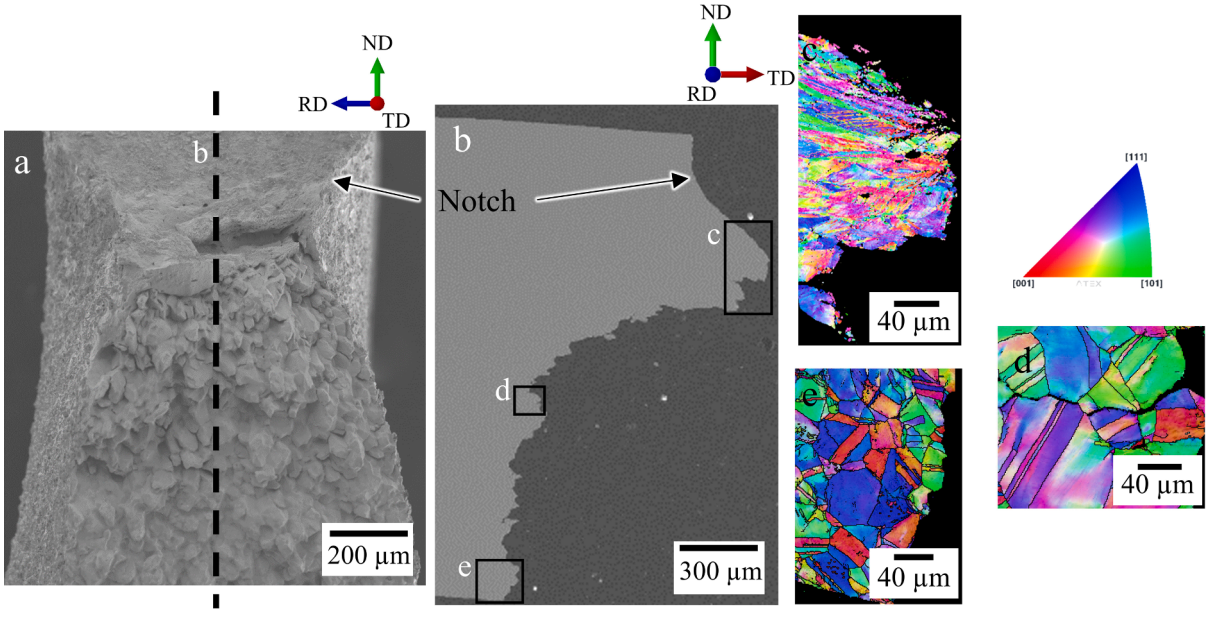

Fig. 8. EBSD analysis on a transversal cut of a fractured Cu-30 %Zn as-received sample tested in contact with the liquid EGaIn using the 3-point bending test with Setup 1 at a 5 mm/min displacement rate.

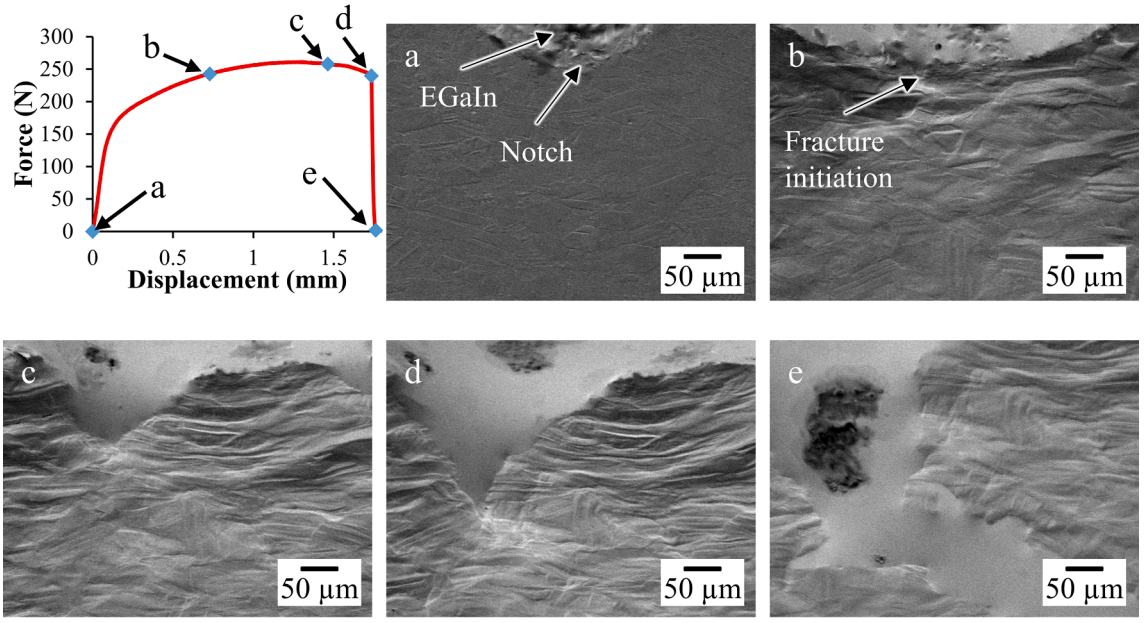

Fig. 9. In situ SEM observations of the fracture of a Cu-30 %Zn as-received sample tested in contact with the liquid EGaIn using the 3-point bending test with Setup 1 at a 0.4 mm/min displacement rate.

3.3. Mechanical testing of Cu-25 %Zn and Cu-20 %Zn alloys in contact with the liquid EGaIn

Moving to α-brasses with less Zn content, Cu-20 %Zn and Cu-25 %Zn alloys were tested at two different displacement rates, in air and in contact with the liquid EGaIn; Fig. 10 shows the respective 3-point bending test curves. The fabrication method of these alloys (detailed in the Methodology section) induced a highly deformed and heterogeneous microstructure, a high yield strength, and a lower displacement to failure. The yield strength varies between the samples, even when tested under the same conditions, probably due to the heterogeneity of the highly deformed microstructure. In any case, the samples tested in contact with the liquid EGaIn present significant differences compared to their counterparts tested in air. Similar to the Cu-30 %Zn samples, there is a sudden force decrease that comes after the point of maximum load. In contrast, the Cu-20 %Zn and Cu-25 %Zn samples present a stable crack growth after the sudden drop of the force followed by a new sudden decrease in the force; this process repeats several times. Considering that a brittle fracture does not need significant energy for its propagation, the sudden decreases in the force would correspond to the propagation of brittle fractures. In contrast, the stable crack growth would correspond to ductile fracture propagation.

Fig. 11 shows the fracture surface of a Cu-20 %Zn sample tested at 5 mm/min in contact with the liquid EGaIn. In this fractography,

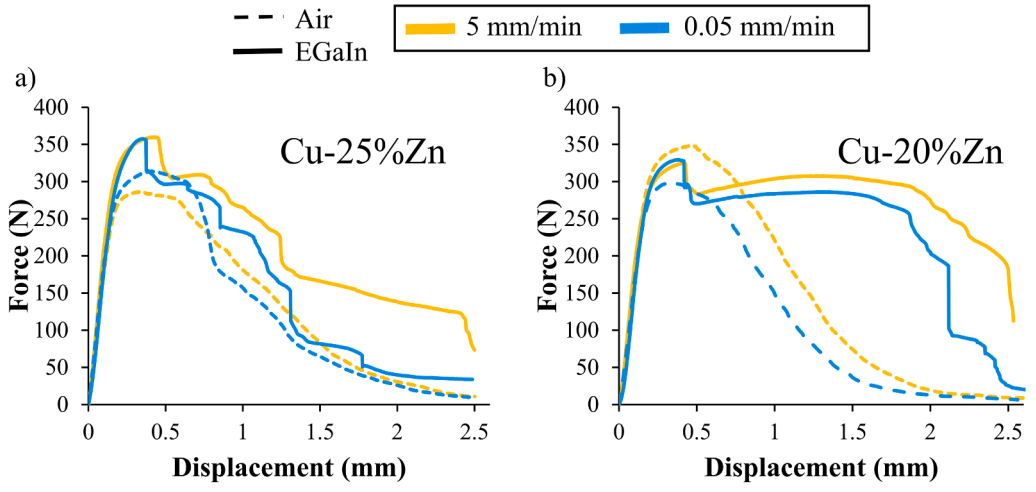

Fig. 10. Force-displacement curves of Cu-20%Zn and Cu-25%Zn as-received samples tested in air and in contact with the liquid EGaIn using the 3-point bending test with Setup 1 at different displacement rates.

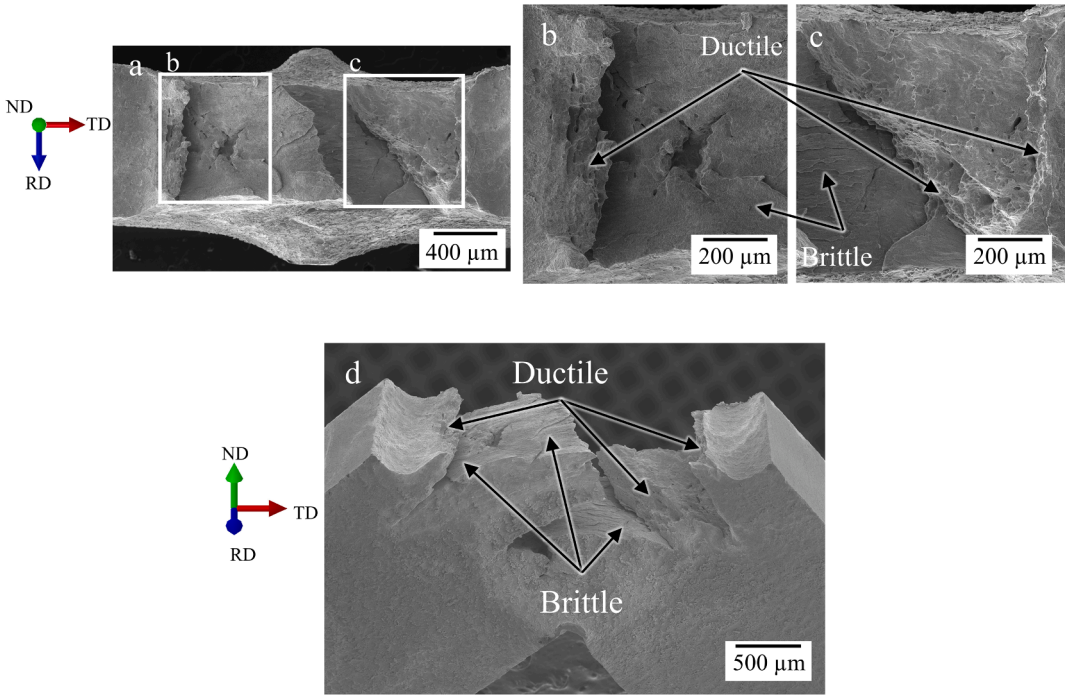

Fig. 11. Fractographies of a Cu-20 %Zn as-received sample tested in contact with the liquid EGaIn using the 3-point bending test with Setup 1 at a 5 mm/min displacement rate.

there is both ductile and brittle behaviour. The brittle behaviour corresponds to the fractures propagating in the plane normal to TD, while the ductile fractures propagate in the plane perpendicular to ND. Moreover, similar to the Cu-30 %Zn samples, the crack initiation is ductile. The ductile fracture presents signs of plasticity and ductility dimples, while the brittle fractures have smooth surfaces. This last could correspond to an intergranular fracture, but due to the deformed microstructure, it is impossible to confirm its nature.

The lateral view in Fig. 11d shows that the brittle fracture propagated in the TD direction until it reached a zone far from the notch where there was no further plastic deformation, and then the fracture propagation stopped. After this, a new ductile fracture appears, which then becomes a brittle fracture that propagates and stops. This series of crack initiations and arrests explains the form of the force–displacement curve.

Additionally, annealed Cu-20 %Zn and Cu-25 %Zn samples were tested; Fig. 12 shows the results of the 3-point bending tests on some of these. In the case of the Cu-25 %Zn annealed at 300 °C, LME appeared only at the higher displacement rate. In comparison, the

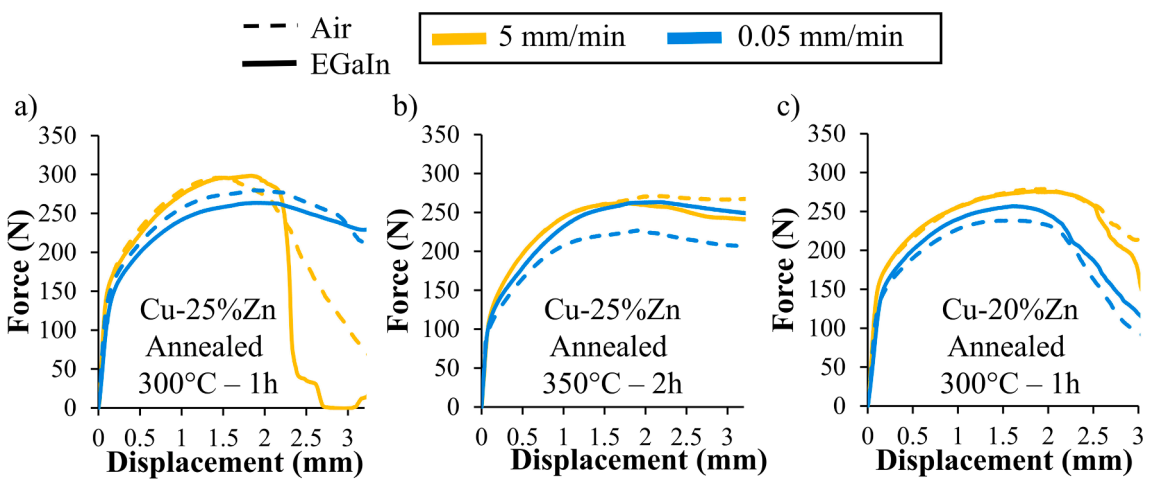

Fig. 12. Force-displacement curves of Cu-20%Zn and Cu-25%Zn samples tested in air and in contact with the liquid EGaIn using the 3-point bending test with Setup 1 at different displacement rates.

Cu-25 %Zn sample annealed at 350 °C did not present any signs of LME under the conditions tested. Similarly, annealing the Cu-20 % Zn alloy at 300 °C eliminated the LME susceptibility under the same conditions. The lack of LME was corroborated by observing the fracture surfaces.

Due to the small material availability, the Cu-20 %Zn and Cu-25 %Zn alloys were not tested with Setup 2.

3.4. Mechanical testing of Cu-15 %Zn in contact with the liquid EGaIn

The Cu-15 %Zn alloy was tested using both setups; Fig. 13 shows the correspondent force–displacement curves. In the case of Setup 1, the curves that correspond to displacement rates of 5, 0.5 and 0.05 mm/min did not present a decrease in the force after reaching the plateau of the maximum load. Indeed, SEM observations of the samples after the tests showed no considerable fracture propagation, both in air and in contact with the liquid EGaIn. This lack of ductile fracture propagation could explain the absence of LME since, in the other alloys, considerable ductile crack propagation always precedes the appearance of the brittle fracture. Moreover, the displacement of these tests is limited to 3 mm because beyond that displacement, due to the small size of the sample, there was contact between the samples and the external parts of the setup. Hence, the tests at these displacement rates cannot conclude if the alloy is sensitive to LME.

Due to the displacement limitation, only the samples tested at 0.005 mm/min presented a decrease in the load, which was the same in air and in contact with the liquid EGaIn, indicating no effect of the liquid EGaIn on the mechanical properties of this alloy. The fracture surface of these samples was observed to corroborate that they presented ductility dimples and no signs of embrittlement.

The displacement limitation can be overridden using a 3-point bending test setup with bigger dimensions, i.e., Setup 2. Fig. 13b and Fig. 13c show that the Cu-15 %Zn samples tested with Setup 2 did present a different behaviour when in contact with the liquid EGaIn. The effect of the liquid EGaIn on the mechanical properties of this alloy appeared only at the higher displacement rates; it consisted of a reduction of the displacement at crack initiation. Contrary to other samples that presented LME, these Cu-15 %Zn did not show a sudden load decrease, indicating that the crack propagation needed significant energy even after the embrittlement. This resembles the fracture behaviour of the Cu-30 %Zn samples annealed for 1.5 h, shown in Fig. 6c.

In summary, for the samples in contact with the liquid EGaIn, the displacement at which the crack initiates depends on the metallurgical state and the displacement rate. At higher displacement rates, the force decreases at lower displacement values, i.e., the fracture initiates sooner under these conditions. The liquid EGaIn has no effect on the mechanical properties at a displacement rate of 1 mm/min. Moreover, when the alloy presents a higher work hardening rate, the displacement at crack initiation when in contact with the liquid EGaIn occurs at lower displacement values. In contrast, the lack of effect at a 1 mm/min displacement rate is maintained.

3.5. Mechanical testing of pure Cu in contact with the liquid EGaIn

The last sample presented here is pure Cu. In both setups, this material presented no signs of LME for any load–displacement curves at the different displacement rates. For instance, the maximum force value stays the same and is reached at the same displacement. Also, the load decrease was steady in all cases, indicating ductile fracture propagation. The fractographies of the samples confirmed the presence of ductile fractures at all displacement rates tested.

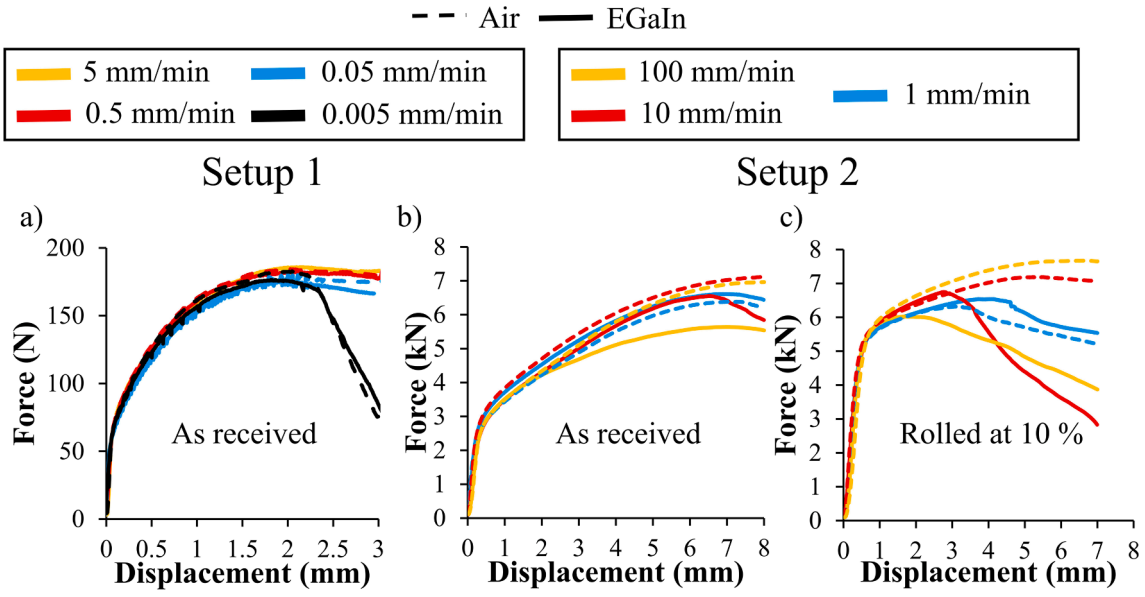

Fig. 13. Force-displacement curves of Cu-15%Zn samples tested in air and in contact with the liquid EGaIn using the 3-point bending test with a) Setup 1 and b-c) Setup2 at different displacement rates.

4. Numerical results

The finite element modelling (FEM) described in the methodology was used to calculate the stress and strain evolution of a Cu-30 % Zn sample during the bending tests corresponding to Setup 1. Fig. 14a compares the load–displacement curves obtained experimentally with that computed by FEM. The computed and experimental curves are similar. A small difference in the slope of the elastic regime arises because the experimental curve is plotted with the displacement imposed on the cross head instead of the real displacement of the supports.

The experimental and simulated curves diverge after a displacement corresponding to the crack initiation since the model used here does not consider any crack initiation. In any case, the value of the simulation was taken at the point of the maximum force (indicated with a point in Fig. 14a). Fig. 14b and c show the computed profiles of maximum principal stress. The stress profile shows that the transition point from negative to positive stress values is around 0.7 mm, far from where the fracture changes its mode. Hence, the transition from a volume in tension to a volume in compression does not cause the change in the fracture behaviour.

Fig. 15 compares the plastic strain calculated with the FEM at the point of maximum force (Fig. 14a) with the fracture of an embrittled Cu-30 %Zn sample (Fig. 8b). This comparison shows that the brittle fracture propagation path matches the zone of the sample with the highest plastic strain values. Moreover, the calculated value of the plastic strain at the bottom of the notch is 1.23, while the value at the zone where the brittle fracture initiates is close to 0.6. These values give a rough indicator of the plastic strain needed for the ductile and brittle fracture initiation. However, to correctly calculate these values, the FEM needs to include fracture initiation and propagation models.

5. Discussion

The α-brasses were found to present LME in contact with the liquid EGaIn. Four essential aspects arise from the results. First, the interface between the α-brasses and the liquid EGaIn, in which there is the formation of the intermetallic $CuGa_2$, must be considered. Second, there are specific ranges of conditions at which there is LME on this system; these were identified. Third, whenever there is LME, the brittle fracture initiation is delayed as the fracture surface presents zones with ductile characteristics at the beginning. Fourth, the path of brittle crack propagation differs from that of ductile crack propagation and follows the zones of higher plastic strain. Finally, analysing these aspects, we discuss the possible mechanisms that lead to the LME of α-brasses in contact with liquid EGaIn.

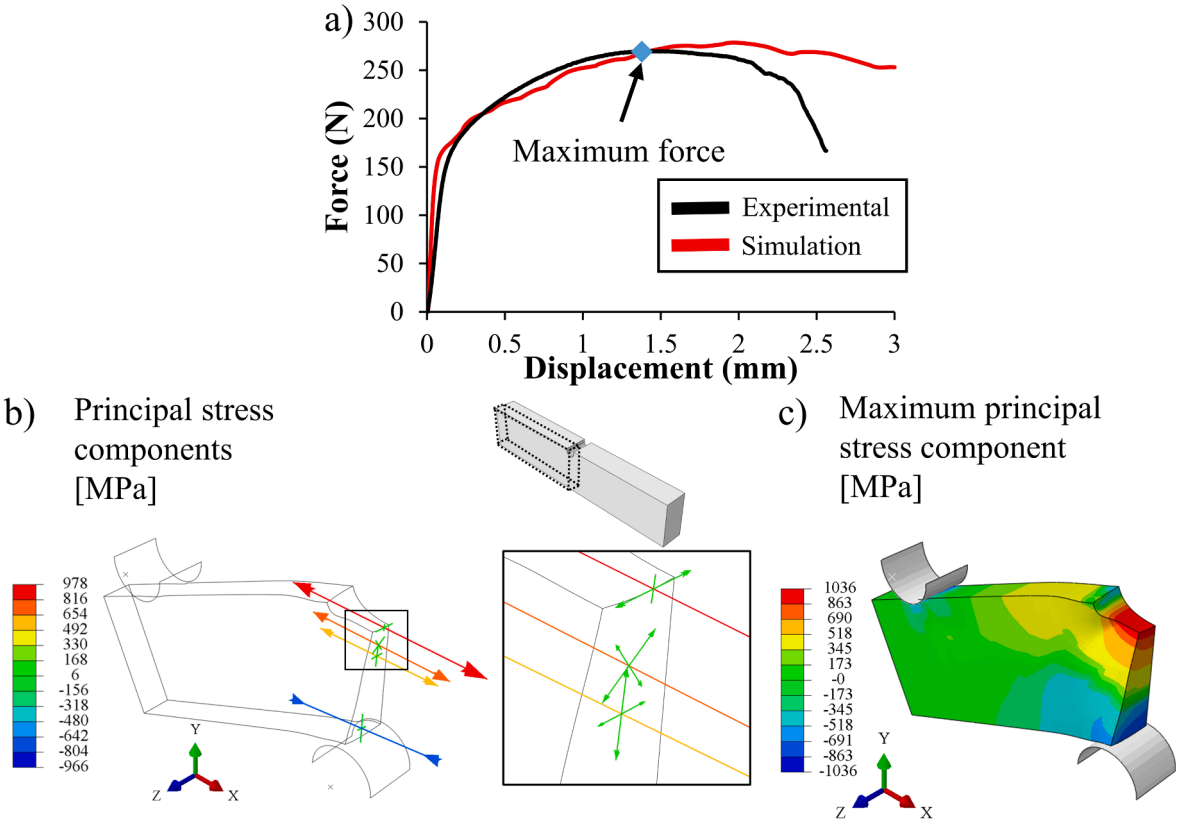

Fig. 14. A) comparison of the calculated and experimental load–displacement curves, b) Principal stress components, and c) Magnitude of the maximum principal stress component of a 3-point bending test Cu-30%Zn specimen tested with Setup 1.

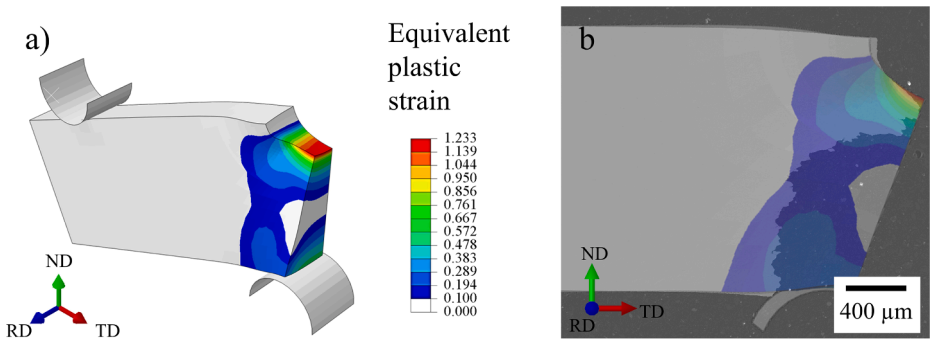

Fig. 15. Comparison of the calculated equivalent plastic strain with the fracture of an embrittled Cu-30 %Zn sample tested using the 3-point bending test with Setup 1 at a 5 mm/min displacement rate.

5.1. Solid/liquid interface

The liquid EGaIn wets partially pure Cu and the α-brasses. This wetting is under the regime of high wettability with contact angle average values below 50°. These values decrease slightly from 49.2 to 35.9° between Cu and Cu-30 %Zn alloy; hence, Zn alloying favours wetting. This tendency matches the fact that the LME sensitivity increases with Zn content. Following the contact with the liquid EGaIn, the Ga reacts with the Cu to form the $CuGa_2$, in accordance with the literature [24,34].

In the case of Fe in contact with liquid Zn, Kang et al. [7] stated that the intermetallics impede the LME when the displacement rate is slow since there is more time for them to form and reduce the exposure of Fe to liquid Zn. In the case of α-brasses in contact with the liquid EGaIn, this behaviour is not followed. For instance, the Cu-30 %Zn alloy presented LME even during the 3-point bending test at displacement rates of 0.005 mm/min, a mechanical test that takes several hours. Due to the morphology of the $CuGa_2$ (Fig. 2), the liquid EGaIn may easily continue to be in contact with the surface of the solid when it forms. Moreover, embrittlement was found to happen after a crack had already occurred (Fig. 9d). Hence, the liquid EGaIn always enters with a fresh surface of the solid independently of the displacement rate of the test.

It is possible to make a rough comparison between the crack propagation rate and the growth rate of the $CuGa_2$ intermetallic by considering the model of Tikhomirova et al. [38]. This model predicts that it takes 1.4×10^6 min to form an intermetallic of 200 µm, roughly the size of the ductile fracture preceding the brittle crack (Fig. 9d). In contrast, the crack propagation rate of 1.1 µm/s at a displacement rate of 0.4 mm/min, calculated previously from Fig. 9, is six orders of magnitude faster than the estimated $CuGa_2$ growth rate. Moreover, the model of Tikhomirova et al. is based on the $CuGa_2$ growth rate on Cu particles at 100 °C, so the growth rate is expected to be even slower at room temperature in bulk α-brasses samples. This makes it unlikely that the $CuGa_2$ intermetallic formation plays a significant role in the LME of α-brasses by the liquid EGaIn.

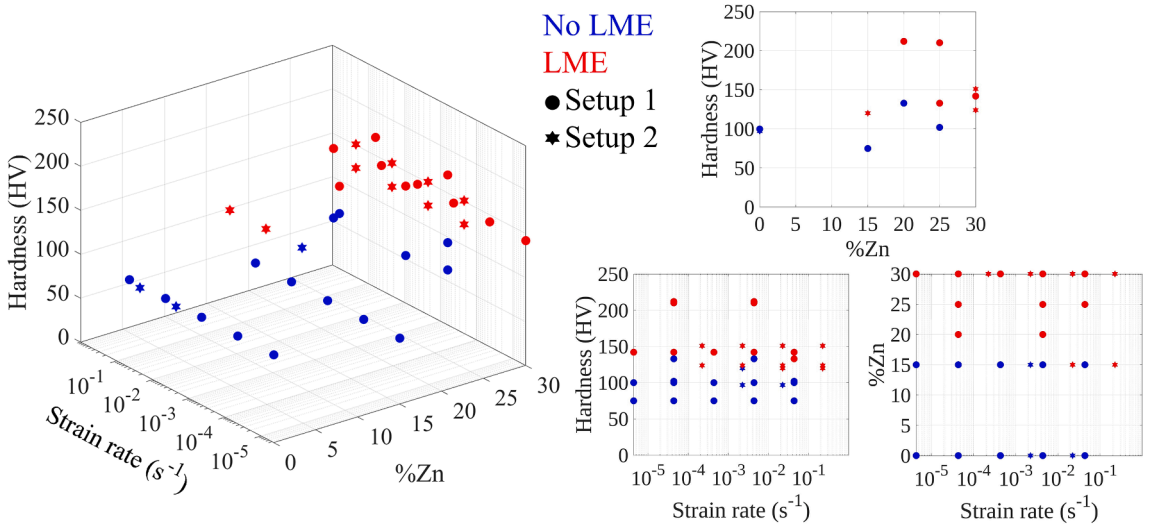

Fig. 16. Schema of the conditions where there was LME (red) or not (blue) for the samples in contact with the liquid EGaIn tested using the 3-point bending test with Setup 1 (dots) and Setup 2 (hexagrams).

5.2. Effect of the parameters on the LME appearance

Three variables influence the LME sensitivity of the α-brass by the liquid EGaIn: the Zn content, the strain rate, and the work hardening rate (hardness). Fig. 16 illustrates how, by increasing any of these parameters, the solid is more sensitive to LME by the liquid EGaIn.

To compare the results of the two different setups, the strain rate was approximated using the analytical formula in Eq. (1):

$$\frac{d\varepsilon}{dt} = \frac{12y}{L^2}\frac{d\delta}{dt} \tag{1}$$

where y is the vertical distance between the centre of the sample and the bottom of the notch, L is the span length, and $\frac{d\delta}{dt}$ corresponds to the displacement rate. This formula is only valid in the elastic regime but allows us to estimate the strain rate order of magnitude for each test. To have an exact value of strain rate, a FEM should be used to calculate the value of the strain rate at the point of fracture, describing the mechanical behaviour of each material at the exact moment of fracture for each of the tests, requiring additional tensile testing and in situ observations, which would be a demanding task. For instance, the FEM of the Cu-30 %Zn was used to calculate the strain rate at the fracture initiation point for a sample tested at 5 mm/min, and it was compared with the analytical formula. The strain rate value from the FEM is 0.031 s^{-1} under the notch, while the value from the analytical formula is 0.044 s^{-1}; hence the approximated strain rate is suitable, as a first step, for comparing the conditions under which LME occurs.

The variables that affect the LME sensitivity of the α-brasses relate closely to the plastic deformation of the solid. The Zn content of the α-brasses strongly influences the dislocation motion since it is responsible for the solid solution strengthening of these alloys and decreases their stacking fault energy (SFE). The work hardening rate of the material directly relates to the dislocation density. When all other microstructural parameters, such as the grain size, are constant, a higher hardness value indicates a higher dislocation density in the solid metal. Whenever the dislocation density increases, the quantity of deformation that the material can accommodate significantly reduces since the other dislocations restrict the dislocation motion, and the dislocation nucleation is limited. Similarly, the strain rate defines how fast the dislocations need to accommodate the plastic deformation.

Regarding the strain rate, it was argued earlier that the $CuGa_2$ intermetallic formation does not seem to affect the LME sensitivity. Moreover, the kinetics of the intermetallic cannot fully explain the strain rate dependency since different alloys with close compositions tested at the same strain rate showed dissimilar LME sensitivities, e.g., Cu-30 %Zn and Cu-25 %Zn (Fig. 5b and Fig. 12a, respectively). It is more likely that the effect of the strain rate relates to its impact on the dislocation motion, which is similar to the Zn-content, i.e., higher strain rates hinder the dislocation movement.

5.3. Brittle fracture initiation

Under the conditions where there is LME, the fracture does not present brittle characteristics at the very beginning; instead, there is a fracture with ductile characteristics. One plausible explanation for this fracture behaviour is that the liquid metal does not enter contact with a suitable grain boundary, so there is no immediate embrittlement. However, the viscosity of the EGaIn is relatively low (1.99×10–3 kg m^{-1} s^{-1}), so it flows easily by capillarity into the crack. This flow was corroborated by the in situ observations; Fig. 9 showed that the liquid EGaIn enters inside the ductile fracture immediately after its formation. Considering that the ductile fracture propagated significantly without any signs of embrittlement and that the sample thickness is 1 mm and the grain size is around 20 μm, the probability of the liquid metal meeting a suitable grain boundary is high.

Similarly, an appealing explanation of the fracture behaviour is the presence of the $CuGa_2$ intermetallic since it may block the contact between the solid and the liquid, impeding the LME. If this was the case, as soon as the ductile fracture appeared, there would be a fresh solid surface under plastic strain in contact with the EGaIn, and under these conditions, LME would have immediately occurred. Yet, it was observed that the ductile fracture propagated slowly to some hundreds of microns (Fig. 9) before the appearance of the brittle fracture.

The fact that the $CuGa_2$ intermetallic does not play a relevant role in the LME may be related to its morphology. As observed in Fig. 2, the intermetallic does not grow uniformly nor compact, so it should be possible for the EGaIn to infiltrate during the deformation of the solid samples. Moreover, like other intermetallics, this intermetallic may be very brittle, so it could break at little strain values, allowing the liquid metal to enter into contact with the solid.

The delay of the brittle fracture could also be explained by the magnitudes of stress concentration and stress triaxiality since the presence of a crack considerably increases these values. Although the stress concentration and the stress triaxiality may have played a role in the LME, their magnitudes were not the only reason for the ductile crack to occur. Otherwise, the brittle fracture could have been initiated immediately after the formation of the first ductile crack, but instead, there was a considerable ductile fracture propagation.

A proposed explanation of the delay of the brittle fracture is the existence of a plastic strain threshold. In this case, even if there is contact between the solid and the liquid, if the solid does not attain this plastic strain or strain hardening value, LME cannot occur; hence, there is a fracture initiation with ductile characteristics. As this ductile fracture propagates, the zone below the fracture accumulates plastic strain until it reaches the threshold value at which the brittle fracture can initiate. Fig. 17 schematises this scenario.

In most cases where there was LME, once the brittle fracture initiated, its propagation occurred rapidly and did not stop. The exceptions occurred when the fracture propagated into a zone where there was no more plastic deformation to drive the fracture propagation. This was observed for the Cu-20 %Zn and Cu-25 %Zn alloys (Fig. 11).

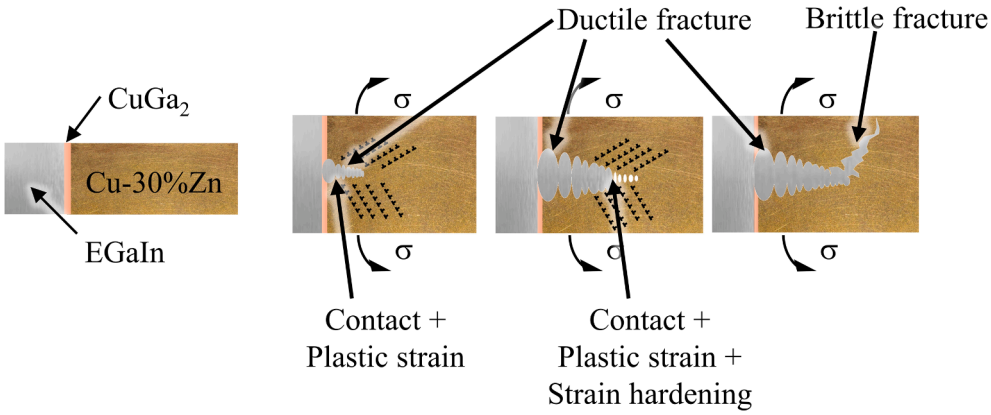

Fig. 17. Schema of the LME of the α-brass in contact with the liquid EGaIn.

5.4. Brittle fracture propagation

Fig. 15 shows that contrary to the ductile fracture that propagates following the path with the higher stress (ND direction), the brittle fracture propagates following the path with the higher plastic strain. These zones would present higher dislocation density and be in accord with the hardness dependence of the LME sensitivity.

The deformation of the grains during the first cracking stage could have also influenced the brittle crack propagation. Fig. 8c shows that the zone around the fracture initiation presents a microstructure with grain elongated in the TD direction. Since the brittle fracture is intergranular, the easiest path for its propagation would be the TD direction; this agrees with the experimental observations. In this case, the change of the crack propagation (Fig. 8b) could be explained by the lack of stress that does not allow the fracture to propagate in that direction, similar to the case of the crack arrest in the case of Cu-%20Zn (Fig. 11). In contrast, on microstructures with equiaxed grains, like for the Cu-30 %Zn (Fig. 8d and Fig. 8e), the brittle fracture can change the direction of its propagation to follow the path with the highest stress, i.e., in the ND direction.

5.5. Mechanisms of LME on α-brasses in contact with the liquid EGaIn

Even if there is a significant dissolution of Cu and Zn into the liquid EGaIn, this dissolution cannot explain the LME since the solid elements cannot dissolve as fast as the brittle crack propagation rate (2.4 mm/s at a displacement rate of 0.4 mm/s). Likewise, the diffusion does not match the fast crack propagation. Moreover, these phenomena do not play a role in the brittle crack initiation since the brittle crack initiation occurs after the initiation and propagation of a ductile fracture. The length of this ductile fracture (approximately 200 μm) is sufficiently long to make any effect of diffusion or dissolution irrelevant. Also, if any time-dependent phenomena would control the LME occurrence, the embrittlement would be enhanced at lower displacement rates. Still, in the system of this study, there is an opposite tendency. In contrast, the adsorption of the liquid metal atoms on the solid surface may modify the dislocation moving towards and from the grain boundaries.

In this system, the LME does not depend only on a stress threshold since this threshold would have been reached just after the first crack appearance. Instead, the strain seems to play an essential role in LME. In this sense, an apparent threshold of plastic strain was present for the brittle fracture to initiate, while its propagation is also favoured by the degree of plastic strain in the sample. It must be noted that the magnitude of plastic strain at the brittle crack initiation is higher than that of the brittle crack propagation. Also, even if plastic deformation plays an important role in LME, the brittle fracture phenomenon does not occur through micro-void coalescence.

In their article, Fernandes and Jones [25] propose that the dislocation mobility is linked with the LME of Cu-30 %Zn and Cu-40 %Zn brasses. They suggest that planar glide promotes the occurrence of LME since this facilitates brittle crack initiation. Also, they propose a relation of the parameters that enhanced LME with their effect on dislocation mobility. It is worth noting that they compared a monophasic alloy with a biphasic alloy, and they did not consider the different contributions to the LME of the two phases in the α-β brasses. Moreover, they used tensile tests, so the lack of crack initiation in the surface may have masked the possible presence of LME.

Their observations accord with those in this work since the parameters that enhanced LME also impact the dislocation mobility and may favour the dislocation movement by planar glide. This is especially relevant in terms of Zn content. Zn additions decrease SFE, enhancing the planar glade; moreover, Zn is in a solid solution, hindering dislocation mobility.

To extend our understanding of LME in α-alloys when in contact with liquid EGaIn, future work could encompass different approaches. Performing dynamic wetting tests can reveal if the contact angle measured in this work corresponds to that of the liquid EGaIn on the $CuGa_2$ intermetallic or the liquid EGaIn on the actual metal or alloy while also allowing the measurement of the angle hysteresis. Additionally, in situ observations of LME phenomena through scanning and transmission electron microscopy would offer valuable insights into the mechanisms at play at the microscale. Conclusions.

The present work studied the liquid metal embrittlement (LME) of α-brasses in contact with the liquid EGaIn. This is a reactive system since there is the formation of the $CuGa_2$ intermetallic. Studying this kind of system can help further understand the LME

phenomenon. Indeed, the literature on LME is centred on non-reactive systems, with the notable example of Fe-Zn. Moreover, the EGaIn is liquid at room temperature, which eases its study and allows for the in situ observations of the phenomenon in a scanning electron microscope (SEM).

The liquid EGaIn wets partially the pure Cu and the α-brass alloys. The wetting is in the regime of high wettability with contact angle values below 50° and a slight tendency to increase the wettability with the Zn content. The α-brasses were found to be sensitive to LME in contact with the liquid EGaIn under a specific range of conditions. The parameters that modify the LME sensitivity are Zn content, strain rate, and work hardening rate; an increase in the values of these parameters is linked with an increase in the LME occurrence.

Whenever there is LME, the samples present a fracture surface with an initial zone with ductile characteristics, i.e., ductility dimples and grain elongation, followed by a large zone with brittle intergranular characteristics. A comparison with a simulation using the finite element method showed that the ductile fracture propagated into the zones with the higher stress. In contrast, the brittle fracture propagated into the zones with the higher plastic deformation.

The formation of the $CuGa_2$ intermetallic does not affect the embrittlement of the α-brasses since it does not impede the contact between the liquid and the solid during its plastic deformation. The delay of the brittle fracture is unrelated to the intermetallic formation; otherwise, the brittle crack would have started as soon as the ductile crack was formed. Instead, the delay seems related to a strain hardening necessary for the material to present brittleness in contact with the liquid EGaIn.

In situ observations using a scanning electron microscope confirmed the introduction of the liquid metal into the fracture along all stages of propagation. Moreover, these observations allowed for identifying the start of the ductile and brittle fractures and estimating their propagation rate.

The parameters that affect the LME are the work hardening rate, the Zn content, and the strain rate; an increase in any of these parameters elevates the LME sensitivity. Moreover, there is a threshold of strain hardening necessary for the brittle crack to initiate, and once it initiated, the brittle fracture follows the path of the highest plastic deformation. The condition that enhances LME points to a role of dislocation mobility on the LME of α-brasses in contact with the liquid EGaIn. The effect of these parameters on the dislocation mobility, i.e., favouring planar glide over wavy glide, may explain the LME occurrence.

In this system, the time-dependent phenomena, such as diffusion, dissolution and reaction, cannot explain the LME. The adsorption of the liquid metal atoms on the surface of the solid possibly affects the dislocation mobility. To achieve a deeper insight into the mechanisms responsible for the LME of the studied system, an experiment with in situ observations at the grain size scale should be made using SEM and TEM.

6. Contribution statement

Marco Ezequiel: Writing – Original Draft, Software, Investigation. **Ingrid Proriol Serre:** Writing – Review & Editing, Methodology, Supervision. **Thierry Auger:** Writing – Review & Editing, Methodology, Supervision. **Eva Héripré:** Writing – Review & Editing, Supervision. **Zehoua Hadjem-Hamouche:** Investigation, Writing – Review & Editing. **Loïc Perrière:** Resources.

Funding

This work was financed by the French National Research Agency (ANR) under the project ANR GauguIn (N° ANR-18-CE08-0009–01) and by our institutes, especially the French National Center for Scientific Research and the University of Lille (France).

CRediT authorship contribution statement

Marco Ezequiel: Writing – original draft, Software, Investigation. **Ingrid Proriol Serre:** Writing – review & editing, Supervision, Methodology. **Thierry Auger:** Writing – review & editing, Supervision, Methodology. **Eva Héripré:** Writing – review & editing, Supervision. **Zehoua Hadjem-Hamouche:** Writing – review & editing, Investigation. **Loïc Perriere:** Resources.

Declaration of competing interest

The authors declare that they have no known competing financial interests or personal relationships that could have appeared to influence the work reported in this paper.

Acknowledgements

The authors thank the Chevreul Institute for its help in the development of this work through the ARCHI-CM project supported by the "Ministère de l'Enseignement Supérieur de la Recherche et de l'Innovation", the region "Hauts-de-France", the ERDF program of the European Union and the "Métropole Européenne de Lille". The authors thank Dr Alexandre Fadel from the Chevreul Institute for his help and his work during the tests with in situ SEM observations, Dr Jean-Baptiste Marijon for the DIC analysis, and Dr Vincent Magnier and the University of Lille for the access to the ABAQUS 6.13 license.

Data Availability

Data are available in the references cited in this article or upon request to the corresponding authors.

References

[1] V.V. Popovich, I.G. Dmukhovskaya, The embrittlement of metals and alloys being deformed in contact with low-melting alloys (a review of foreign literature), Sov. Mater. Sci. 23 (1988) 535–544, https://doi.org/10.1007/BF01151882.
[2] M.H. Kamdar, The occurrence of liquid-metal embrittlement, Physica Status Solidi (a) 4 (1971) 225–233, https://doi.org/10.1002/pssa.2210040123.
[3] T. Auger, J.-B. Vogt, I. Proriol Serre, Liquid Metal Embrittlement, in: Mechanics - Microstructure - Corrosion Coupling, Elsevier, 2019: pp. 507–534. doi: 10.1016/B978-1-78548-309-7.50022-3.
[4] M.H. Razmpoosh, C. DiGiovanni, Y.N. Zhou, E. Biro, Pathway to understand liquid metal embrittlement (LME) in Fe-Zn couple: From fundamentals toward application, Prog Mater Sci 121 (2021) 100798, https://doi.org/10.1016/j.pmatsci.2021.100798.
[5] E.E. Glickman, Multiscale Phenomena in Plasticity: From Experiments to Phenomenology, Modelling and Materials Engineering, Springer, Netherlands, Dordrecht (2000), https://doi.org/10.1007/978-94-011-4048-5.
[6] H. Lee, M.C. Jo, S.S. Sohn, S.-H. Kim, T. Song, S.-K. Kim, H.S. Kim, N.J. Kim, S. Lee, Microstructural evolution of liquid metal embrittlement in resistance-spot-welded galvanized TWinning-Induced Plasticity (TWIP) steel sheets, Mater Charact 147 (2019) 233–241, https://doi.org/10.1016/j.matchar.2018.11.008.
[7] J.-H. Kang, S.-H. Hong, J. Kim, S.-J. Kim, Zn-induced liquid metal embrittlement of galvanized high-Mn steel: Strain-rate dependency, Mater. Sci. Eng. A 793 (2020) 139996, https://doi.org/10.1016/j.msea.2020.139996.
[8] K.-F. Nilsson, A. Hojna, Overview of Mechanisms & Models for Liquid Metal Embrittlement and Future Directions, Eur 29437 En (2018) 1–26. doi: 10.2760/017392.
[9] D.G. Kolman, A review of recent advances in the understanding of liquid metal embrittlement, Corrosion 75 (2019) 42–57, https://doi.org/10.5006/2904.
[10] J.E. Norkett, M.D. Dickey, V.M. Miller, A Review of Liquid Metal Embrittlement: Cracking Open the Disparate Mechanisms, Metall. Mater. Trans. A 52 (2021) 2158–2172, https://doi.org/10.1007/s11661-021-06256-y.
[11] B. Joseph, M. Picat, F. Barbier, Liquid metal embrittlement: A state-of-the-art appraisal, EPJ Applied Physics 5 (1999) 19–31, https://doi.org/10.1051/epjap:1999108.
[12] P.J.L. Fernandes, D.R.H. Jones, Specificity in liquid metal induced embrittlement, Eng Fail Anal 3 (1996) 299–302, https://doi.org/10.1016/S1350-6307(96)00022-2.
[13] M.H. Kamdar, Fracture in liquid metal environments, Elsevier, 1984, pp. 3851–3875, in: Fracture 84,.
[14] B. Long, Z. Tong, F. Gröschel, Y. Dai, Liquid Pb–Bi embrittlement effects on the T91 steel after different heat treatments, J. Nucl. Mater. 377 (2008) 219–224, https://doi.org/10.1016/j.jnucmat.2008.02.050.
[15] M.G. Nicholas, C.F. Old, Review Liquid metal embrittlement, J Mater Sci 14 (1979) 1–18.
[16] E.É. Glikman, Y.V. Goryunov, V.M. Demin, K.Y. Sarychev, Kinetics and mechanism of copper fracture during deformation in surface-active baths, Sov. Phys. J. 19 (1976) 839–843, https://doi.org/10.1007/BF00892898.
[17] Z. Hamouche-Hadjem, T. Auger, I. Guillot, D. Gorse, Susceptibility to LME of 316L and T91 steels by LBE: Effect of strain rate, J. Nucl. Mater. 376 (2008) 317–321, https://doi.org/10.1016/j.jnucmat.2008.02.031.
[18] C. Ye, J.-B. Vogt, I. Proriol Serre, Liquid metal embrittlement of the T91 steel in lead bismuth eutectic: The role of loading rate and of the oxygen content in the liquid metal, Mater. Sci. Eng. A 608 (2014) 242–248, https://doi.org/10.1016/j.msea.2014.04.082.
[19] S.P. Lynch, Metal-induced embrittlement of materials, Mater Charact 28 (1992) 279–289, https://doi.org/10.1016/1044-5803(92)90017-C.
[20] P. Gordon, H.H. An, The mechanisms of crack initiation and crack propagation in metal-induced embrittlement of metals, Metall. Trans. A 13 (1982) 457–472, https://doi.org/10.1007/BF02643354.
[21] P.H. Au-Yeung, J.T. Lukowski, L.A. Heldt, C.L. White, An auger spectrometric study of the crack tip surface chemistry for liquid metal embrittlement: Beta brass embrittled by gallium, Scripta Metallurgica et Materiala 24 (1990) 95–100, https://doi.org/10.1016/0956-716X(90)90573-Y.
[22] R.E. Clegg, D.R.H. Jones, Liquid metal embrittlement of tensile specimens of En19 steel by tin, Eng Fail Anal 10 (2003) 119–130, https://doi.org/10.1016/S1350-6307(02)00024-9.
[23] E.E. Glikman, Y.V. Goryunov, Mechanism of embrittlement by liquid metals and other manifestations of the Rebinder effect in metal systems, Sov. Mater. Sci. 14 (1979) 355–364, https://doi.org/10.1007/BF01154710.
[24] J. Froemel, M. Baum, M. Wiemer, T. Gessner, Low-Temperature Wafer Bonding Using Solid-Liquid Inter-Diffusion Mechanism, J. Microelectromech. Syst. 24 (2015) 1973–1980, https://doi.org/10.1109/JMEMS.2015.2455340.
[25] P.J.L. Fernandes, D.R.H. Jones, The effects of microstructure on crack initiation in liquid-metal environments, Eng Fail Anal 4 (1997) 195–204, https://doi.org/10.1016/s1350-6307(97)00010-1.
[26] J.T. Lukowski, D.B. Kasul, L.A. Heldt, C.L. White, Discontinuous crack propagation in Ga induced liquid metal embrittlement of β-brass, Scripta Metallurgica et Materiala 24 (1990) 1959–1964, https://doi.org/10.1016/0956-716X(90)90058-O.
[27] Q. Xu, N. Oudalov, Q. Guo, H.M. Jaeger, E. Brown, Effect of oxidation on the mechanical properties of liquid gallium and eutectic gallium-indium, Phys. Fluids 24 (2012) 063101, https://doi.org/10.1063/1.4724313.
[28] D. Kim, P. Thissen, G. Viner, D.W. Lee, W. Choi, Y.J. Chabal, J.B. Lee, Recovery of nonwetting characteristics by surface modification of gallium-based liquid metal droplets using hydrochloric acid vapor, ACS Appl Mater Interfaces 5 (2013) 179–185, https://doi.org/10.1021/am302357t.
[29] Y. Cui, F. Liang, Z. Yang, S. Xu, X. Zhao, Y. Ding, Z. Lin, J. Liu, Metallic Bond-Enabled Wetting Behavior at the Liquid Ga/CuGa2 Interfaces, ACS Appl Mater Interfaces 10 (2018) 9203–9210, https://doi.org/10.1021/acsami.8b00009.
[30] D. Whitehouse, Surfaces and Their Measurement, Gulf Professional Publishing (2002), https://doi.org/10.1016/B978-1-903996-01-0.X5000-2.
[31] J. Schindelin, I. Arganda-Carreras, E. Frise, V. Kaynig, M. Longair, T. Pietzsch, S. Preibisch, C. Rueden, S. Saalfeld, B. Schmid, J.-Y. Tinevez, D.J. White, V. Hartenstein, K. Eliceiri, P. Tomancak, A. Cardona, Fiji: an open-source platform for biological-image analysis, Nat Methods 9 (2012) 676–682, https://doi.org/10.1038/nmeth.2019.
[32] M. Brugnara, Contact Angle, (2004). https://imagej.net/ij/plugins/contact-angle.html (accessed December 1, 2020).
[33] S. Hemery, C. Berdin, T. Auger, M. Bourhi, Modelling of liquid sodium induced crack propagation in T91 martensitic steel: Competition with ductile fracture, J. Nucl. Mater. 481 (2016) 24–32, https://doi.org/10.1016/j.jnucmat.2016.09.009.
[34] S. Liu, K. Sweatman, S. McDonald, K. Nogita, Ga-based alloys in microelectronic interconnects: A review, Materials 11 (2018) 1–20, https://doi.org/10.3390/ma11081384.
[35] M. Ezequiel, Mechanisms of liquid metal embrittlement of Cu-Zn alloys by the liquid Ga-In eutectic, University of Lille, 2023. Doctoral dissertation,.
[36] E. Martínez-Pañeda, I.I. Cuesta, I. Peñuelas, A. Díaz, J.M. Alegre, Damage modeling in Small Punch Test specimens, Theor. Appl. Fract. Mech. 86 (2016) 51–60, https://doi.org/10.1016/j.tafmec.2016.09.002.
[37] D.S. SIMULIA, 23.2.9 Porous Metal Plasticity, in: ABAQUS 6.13 User's Manual, 2013.
[38] O.I. Tikhomirova, M.V. Pikunov, L.P. Ruzinov, I.D. Marchukova, Interaction of liquid gallium with copper, Sov. Mater. Sci. 5 (1972) 586–590, https://doi.org/10.1007/BF00721171.